Electron Heat Transport in Low Density H-mode Plasmas with dominant Ion Heating in ASDEX Upgrade

A. Manini, F. Ryter, J. Stober, C. Angioni, K. K. Kirov, F. Leuterer, C. Maggi, W. Suttrop, D. Wagner the ASDEX Upgrade Team

Max-Planck-Institut für Plasmaphysik, EURATOM Association, 85748 Garching, Germany

Introduction and experimental conditions

Understanding energy transport in fusion plasmas is a crucial issue for predicting future devices because it directly determines the performance. Recently, considerable progress has been made, especially in regimes with dominant electron heating [1,2]. Studies in steady state together with comparison with empirical and physics-based modelling, in low density L-mode plasmas with on- and off-axis electron cyclotron heating (ECH), suggest that the electron heat transport is governed by turbulence with a threshold in $\nabla T_e / T_e$. This is in agreement with the main candidates that are supposed to cause the anomalous transport, the coupled trapped electron mode and ion temperature gradient (TEM/ITG) driven turbulence, and it is confirmed by transient transport studies performed by using modulated ECH (MECH). It must be underlined that the "normal" working point for these kind of plasmas (L-mode, low density, strong electron heating, $T_e \gg T_i$) is above the critical gradient and that the electron heat transport does exhibit a strong stiffness under such conditions [1].

In contrast, the electron heat transport in plasmas with dominant ion heating has not yet been investigated in detail and this is the aim of this paper. For these studies, improved H-mode (sawtooth free) plasmas [3] with low coupling between electrons and ions have been used. A series of low density H-mode discharges have been performed in which the dominant ion heating is provided by 5 MW neutral beam injection (NBI). Under these conditions the power delivered to the ions is approximately 80%, the remaining 20% (approximately 1 MW) to the electrons. The power in the electron channel can be more than doubled by applying up to the available 2.0 MW of ECH, while the power in the ion channel is not changed significantly. The ECH power is partly modulated so that power balance analysis can be completed with transient studies. Two series of discharges have been performed: one with a higher average electron density of $\bar{n}_e \cong 5.2 \cdot 10^{19} m^{-3}$, a second one with lower $\bar{n}_e \cong 4.5 \cdot 10^{19} m^{-3}$.

All these discharges present two stationary phases, one with NBI only and a second one in which ECH is applied, with the power deposition location ρ_{dep} being on- ($0.1 < \rho_{dep} < 0.2$) or off-axis ($0.35 < \rho_{dep} < 0.55$). The MECH configuration is 50% duty cycle square wave, with frequency $\nu_{MECH} = 38.47 Hz$ and a total average power of 0.4-1.4 MW.

Experimental results

Figure 1 shows the electron and ion temperature profiles for two off-axis ECH heated discharges in the cases of higher and lower electron density. The different symbols represent the experimental observations, as measured by electron cyclotron emission (ECE) for the electron temperature T_e, and charge exchange recombination spectroscopy (CXRS) for the ion temperature T_i.

Several remarks can be made. Very peaked ion temperatures are obtained for the lower density discharges, typically if the averaged electron density is lower than approximately $5 \cdot 10^{19} m^{-3}$. It is also observed that the ion temperature drops significantly in the core as the ECH is turned on. This effect is weaker for the higher density discharges, but where the initial T_i is also lower. In case of on-axis heating, not shown here, the variation in T_i is even more dramatic ($\Delta T_i \sim 40\%$) and it drops to the T_e-level. Considering the electrons, when heating on-axis, T_e increases in the core region ($\rho_t < 0.3$). On the contrary, when the ECH heating is applied off-axis, the T_e profiles basically do not move. A change of approximately 10% in T_e
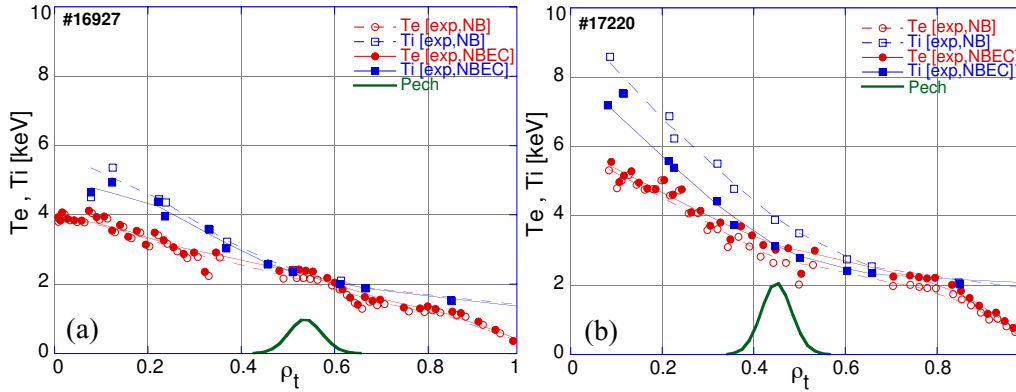
Figure 1. Electron and ion temperature profiles during the NBI-only phase and during the NBI+ECH phase for (a) higher and (b) lower electron density.

is found at low density, but both ∇T_e and $\nabla T_e / T_e$ variations are smaller than 10%. This observation is astonishing considering that the heat flux in the electron channel is increased by a factor which varies between 1.6 for the higher density discharges, to more than 2 for the lower density ones: in practice, the strong ECH power does not produce any T_e variation at the edge and it appears to be expelled from the plasma very rapidly. This is an indication that the electron temperature profiles might be strongly resilient. The reaction of the electron density at the turning on of the ECH, for the higher density cases, is not significant, except for a region inside $\rho_t \sim 0.4$ where the density seems to slightly decrease. For more details we refer to a companion paper [4].

Experimental transport analysis
The power balance diffusivity is as usual given by $\chi_j^{PB} = -q_j / (n_j \cdot \nabla T_j)$ (j related to the species). Considering the ions, the analysis shows that by applying the ECH, q_i increases by less than 15%, while the heat diffusivity χ_i^{PB} increases significantly over the whole radius. Since q_i is not significantly changed by the ECH, the χ_i^{PB} variations are related to the changes in ∇T_i. $\nabla T_i / T_i$ always decreases inside $\rho_t \sim 0.4$ and does not vary outside $\rho_t \sim 0.4$ for the high density cases, while it increases outside $\rho_t \sim 0.4$ for the low density discharges. Considering the electrons, q_e is basically doubled for $\rho > \rho_{dep}$, while it remains unchanged for $\rho < \rho_{dep}$. In all discharges the heat diffusivity χ_e^{PB} is strongly increased only for $\rho > \rho_{dep}$, while $\nabla T_e / T_e$ remains unchanged outside $\rho_t \sim 0.4$. Both n_e and ∇T_e are not significantly modified while q_e is doubled, hence the increase of χ_e^{PB} is driven by the variations in the electron heat flux. These observations indicate resilient electron temperature profiles for the region outside $\rho_t \sim 0.4$.
The analysis of the modulated part of the discharge is carried out as in [5] which yields the perturbative electron heat pulse diffusivity $\chi_e^{HP} = \chi_e^{PB} + \partial \chi_e / \partial \nabla T_e \cdot \nabla T_e$. The modulated data is extracted by Fourier transform and χ_e^{HP} is deduced from amplitude and phase profiles using a slab model [5] corrected for cylindrical geometry [6]. Figure 2 (a,b) shows amplitude and phase profiles for a high density, off-axis MECH discharge. It is interesting to observe the presence of two radii at which an important change in transport occurs, the first one at $\rho_t \sim 0.2$, the second one at $\rho_t \sim 0.43$ ($\rho_{dep} = 0.35$). While the first change might be related to a flat shear in region 1, the second change is related to something else. Figure 2 (c) shows the dependence of χ_e on $\nabla T_e / T_e$: gradient lengths and heat diffusivity are measured for two pairs of discharges, one of each having the MECH on-axis, the other having it off-axis. This allows the determination of χ_e^{PB} and χ_e^{HP} in the "common" region laying between the two deposition locations. From this figure, a critical gradient length can be determined for $\nabla T_e / T_e \cong 2.8 \text{ m}^{-1}$. Measuring this parameter at $\rho_t \sim 0.43$ for the discharge analysed in (a,b) gives $\nabla T_e / T_e \cong 2.9 \text{ m}^{-1}$, a value which is very close to the critical gradient. Figures 2 (a,b,c)
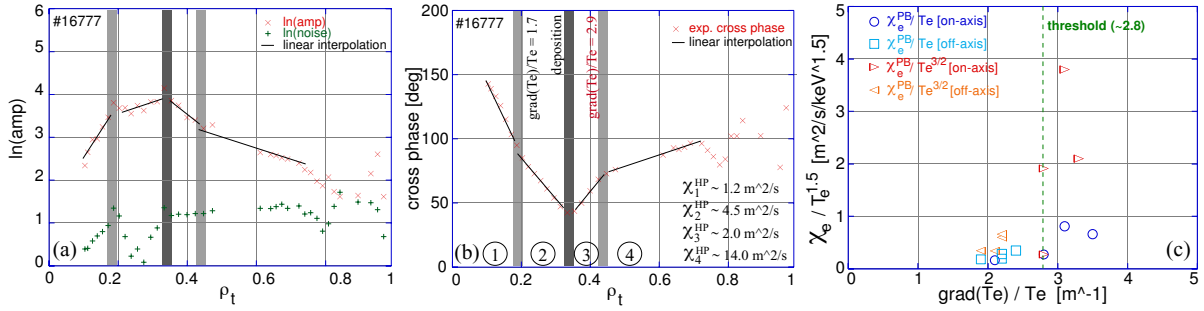
Figure 2. Comparison of (a) amplitude and (b) phase profiles response at the fundamental MECH frequency of 38.47Hz for a high density, off-axis MECH discharge (#16777). (c) Experimental heat diffusivity dependence on the gradient length (data taken at $\rho = 0.3$ and $\rho = 0.45$ respectively).

indicate that outside $\rho_t \sim 0.4$ the T_e profiles are resilient. Applying the same analysis to a pair of discharges performed more on-axis and measuring gradient lengths and χ_e at $\rho_t \sim 0.2$ indicate on the other hand non resilient T_e profiles in the centre.

Modelling

Simulations with two physics based transport models, Weiland [7] and GLF23 [8], have been performed. Both models are fluid models in which transport is calculated based on ITG and TEM physics. For these discharges, the ITG physics of the models is important, since the ion temperature is higher than the electron temperature. For these models, the boundary conditions have been set at $\rho_t = 0.8$. An empirical model based on a critical gradient length where the electron diffusivity is given by $\chi_e = \chi_0 + q\lambda T_e^{3/2}(\nabla T_e/T_e - \kappa)H(\nabla T_e/T_e - \kappa)$ [9] has also been used. q is the safety factor, λ and κ are coefficients to be adjusted and H is the Heaviside function. The factor $T_e^{3/2}$ takes into account the Gyro-Bohm dependence expected for transport driven by micro-turbulence (here, boundary conditions at $\rho_t = 0.9$).
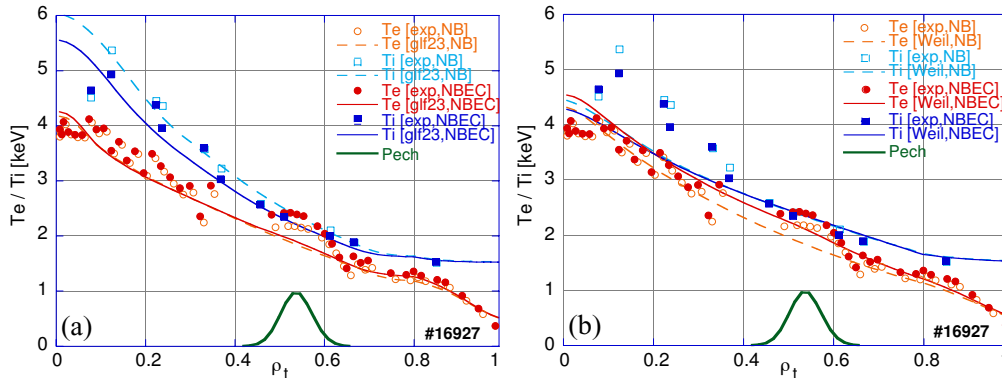

Figure 3. Electron and ion temperature profiles: simulations using the GLF23 (a) and Weiland (b) transport models. Comparison between models and experiments for an off-axis high density discharge.

Figure 3 shows the comparison between experimental and modelled electron and ion temperature profiles obtained by simulating a higher density, off-axis MECH discharge in steady state. The GLF23 model reproduces correctly both electron and ion temperatures. The Weiland model underestimates both electron and ion temperatures inside $\rho_t \sim 0.4$, which indicates that the transport is overestimated. For the lower density discharges (not shown here), neither the Weiland nor the GLF23 models are capable of reproducing the peaked profiles in the region inside $\rho_t < 0.4$. Figure 4 shows the comparison of the experimental and modelled modulation data with the three models. The fit with the analytical model has been obtained with $\kappa = 2.8$ m^{-1}, which is slightly higher than the value found ($\kappa = 2.3$ m^{-1}) by studies previously performed in mostly electron-heated plasmas with $T_e \gg T_i$, $\lambda q = 0.8$, which is approximately a factor of 2 higher than the value previously found [1] and
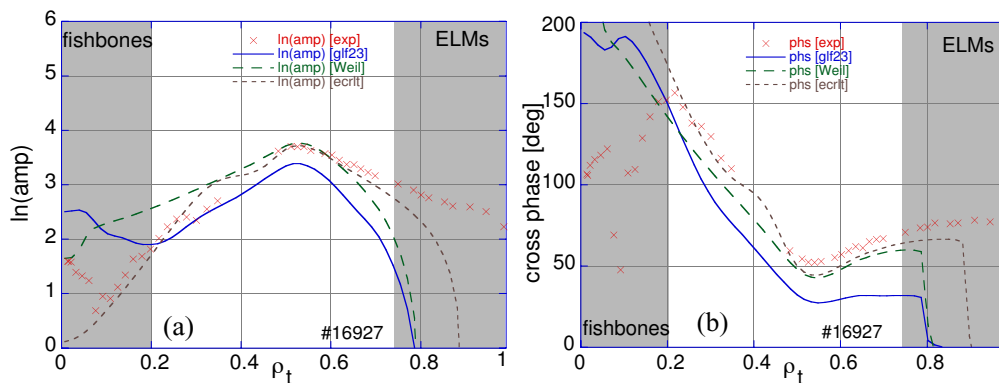
Figure 4. Comparison of amplitude (a) and phase (b) profiles determined by simulating the MECH part of the discharge with the GLF23, Weiland and analytical models.

$\chi_0 = 0.3\ m^2/s$. For $\rho_t < 0.3$ (fishbones in the centre) and $\rho_t > 0.75$ (ELM's induced perturbation from the edge) the modulation profiles are not fully reliable because of the poor signal-to-noise ratio. Despite the fact that for steady state GLF23 shows the best results for both ion and electron temperature profiles, for the MECH it gives worse Fourier amplitude and phase profiles. The Weiland model shows rather good modulation profiles, though with an overestimation of the transport towards the centre.

Conclusions

The experiments performed to study the electron transport in a mostly ion-heated plasma point out an important density dependence, especially for the ion temperature. In the lower density cases, the ion temperature profile strongly peaks in the NBI-only phase, while it collapses when the ECH is turned on. This effect is much weaker in the higher density cases. The electron temperature profiles: when the ECH is turned on, the electron heat flux is increased by a factor 1.6 to above 2, while the gradients remain basically unchanged, especially for the off-axis discharges. The electron heat diffusivity linearly increases with the increasing flux. The MECH transient analysis shows that the electron temperature profiles are very close to the critical gradient region and that they appear to be resilient outside $\rho_t \sim 0.4$. Comparison with transport models shows good agreement in steady state with the GLF23 model for the higher density cases, while both Weiland and GLF23 are not in agreement for the lower density discharges in the central part of the plasma.

Acknowledgements

Bibliography
[1] F. Ryter et al., EX/C4-2Ra, 19th IAEA Fusion Energy Conference (2002), Lyon, France
[2] G. Tardini et al., Nuclear Fusion **42** (2002) L11
[3] A.C.C. Sips, Plasma Physics and Controlled Fusion **44** (2002) B69
[4] C. Angioni et al., this conference, O-3.3A (P-3.87)
[5] N.J. Lopes Cardozo et al., Plasma Physics and Controlled Fusion **37** (1995) 799
[6] A. Jacchia et al., Phys. Fluids **B3** (1991) 3033
[7] J. Weiland et al., Nuclear Fusion **29** (1989) 1810
[8] R.E. Waltz et al., Plasma Physics and Controlled Fusion **38** (1996) 1743
[9] F. Imbeaux et al., Plasma Physics and Controlled Fusion **43** (2001) 1503